九州大学学術情報リポジトリ
Kyushu University Institutional Repository

Effect of hydrogen on creep properties of pure iron

Wada, Kentaro
Graduate School of Mechanical Engineering, Kyushu University

Kubota, Masanobu
International Institute for Carbon-Neutral Energy Research (WPI-I2CNER), Kyushu University

Vijayvargia, Kshitij
International Institute for Carbon-Neutral Energy Research (WPI-I2CNER), Kyushu University

Dadfarnia, Mohsen
International Institute for Carbon-Neutral Energy Research (WPI-I2CNER), Kyushu University

他

https://hdl.handle.net/2324/7450737

出版情報：ISIJ International, 2026. Iron and Steel Institute of Japan
バージョン：
権利関係：Creative Commons Attribution 4.0 International

KYUSHU UNIVERSITY

Effect of hydrogen on creep properties of pure iron

Kentaro WADA,* Masanobu KUBOTA,* Kshitij VIJAYVARGIA,
Mohsen DADFARNIA, Toshihiro TSUCHIYAMA, Petros SOFRONIS,
Reiner KIRCHHEIM, Cynthia A.VOLKERT, Arnaud MACADRE,
Ryosuke KOMODA, Lin TIAN and Juan SHANG

* Corresponding author. E-mail: wada.kentarou.226@s.kyushu-u.ac.jp (K. Wada)
kubota.masanobu.304@m.kyushu-u.ac.jp (M. Kubota)

Received date: June 8, 2026
Accepted date: October 26, 2026
Advance published date: November 4, 2026

DOI: https://doi.org/10.2355/isijinternational.ISIJINT-2026-158

Please cite this article as:

K. WADA, M. KUBOTA, K. VIJAYVARGIA, M. DADFARNIA,
T. TSUCHIYAMA, P. SOFRONIS, R. KIRCHHEIM, C. A.VOLKERT,
A. MACADRE, R. KOMODA, L. TIAN and J. SHANG: *ISIJ Int.*, (2026),
https://doi.org/10.2355/isijinternational.ISIJINT-2026-158



© 2026 The Iron and Steel Institute of Japan. This is an open access article under the terms of the Creative Commons Attribution license (https://creativecommons.org/licenses/by/4.0/).

“ISIJ International” Application Form (Title Page of Manuscripts)

＊Notes on entry:
For items with several options, select one and replace the "○" with a "●".

Fill-in Date	2026/05/21
Title of submitted manuscript	Effect of hydrogen on creep properties of pure iron
Manuscript type	● Regular article ○ Review article ○ Short article ○ Note
【Domestic only】 Reprinted from Tetsu-to-Hagané	○ Yes (Vol._____, No._____, pp._____-_____.) ● No

No.	Full name of every author	ORCID iD (Note*)	Affiliation	Address and E-Mail
Example	Tarou YAMADA	0000-0002-6135-9194	Department of Engineering and Applied Sciences, Faculty of Science and Technology, University of Tekko	3-2-10 Nihonbashi-Kayabacho, Chuo-ku, Tokyo 103-0025 Japan yamada@tetsudai.ac.jp
A 1	Kentaro WADA	0009-0002-9395-4139	Graduate School of Mechanical Engineering, Kyushu University	744 Motooka, Nishi-ku, Fukuoka, Fukuoka wada.kentarou.226@s.kyushu-u.ac.jp
A 2	Masanobu KUBOTA	0000-0001-5100-0762	International Institute for Carbon-Neutral Energy Research (WPI-I2CNER), Kyushu University and Center for Energy Systems Design (CESD), International	744 Motooka, Nishi-ku, Fukuoka, Fukuoka kubota.masanobu.304@m.kyushu-u.ac.jp

			Institute for Carbon-Neutral Energy Research (WPI-I2CNER), Kyushu University,	
A 3	Kshitij VIJAYVARGIA	0009-0003-3759-7947	Department of Mechanical Science and Engineering, University of Illinois at Urbana Champaign and International Institute for Carbon-Neutral Energy Research (WPI-I2CNER), Kyushu University, 744 Motooka, Nishi-ku, Fukuoka, Fukuoka, 819-0395, Japan	1206 West Green Street, Urbana, IL, 61801, USA kv11@illinois.edu
A 4	Mohsen DADFARNIA	0000-0002-5218-971X	Department of Mechanical Engineering, Seattle University and International Institute for Carbon-Neutral Energy Research (WPI-I2CNER), Kyushu University	901 12th Ave, Seattle, WA, 98122-1090, USA dadfarniamoh@seattleu.edu
A5	Toshihiro TSUCHIYAMA	0000-0002-7944-5023	Department of Materials Science and Engineering, Kyushu University and International Institute for Carbon-Neutral Energy Research (WPI-I2CNER), Kyushu University	744 Motooka, Nishi-ku, Fukuoka, Fukuoka, 819-0395, Japan tsuchiyama.toshihiro.178@m.kyushu-u.ac.jp

No.	Full name of every author	ORCID iD (Note2)	Affiliation	Address and E-Mail
A6	Petros SOFRONIS	0000-0002-1891-6928	Department of Mechanical Science and Engineering, University of Illinois at Urbana Champaign and International Institute for Carbon-Neutral Energy Research (WPI-I2CNER), Kyushu University	1206 West Green Street, Urbana, IL, 61801, USA sofronis@illinois.edu
A7	Reiner KIRCHHEIM	0000-0003-2517-8342	Institute of Materials Physics, Georg-August-University of Göttingen and International Institute for Carbon-Neutral Energy Research (WPI-I2CNER), Kyushu University	Friedrich-Hund-Platz 1, 37077 Göttingen, Germany rkirchh@gwdg.de
A8	Cynthia A.VOLKERT	0000-0001-6676-8758	Institute of Materials Physics, Georg-August-University of Göttingen and International Institute for Carbon-Neutral Energy Research (WPI-I2CNER), Kyushu University	Friedrich-Hund-Platz 1, 37077 Göttingen, Germany cynthia.volkert@phys.uni-goettingen.de
A9	Arnaud MACADRE		Department of Mechanical Engineering, Yamaguchi University and International	Tokiwadai 2-16-1, Yamaguchi-ken, Ube-shi, 755-8611, Japan

			Institute for Carbon-Neutral Energy Research (WPI-I2CNER), Kyushu University	macadre@yamaguchi-u.ac.jp
A10	Ryosuke KOMODA	0000-0001-5322-6626	Department of Engineering, Kyushu Institute of Technology and International Institute for Carbon-Neutral Energy Research (WPI-I2CNER), Kyushu University	1-1 Sensui-cho, Tobata-ku, Kitakyushu, Fukuoka, 804-8550, Japan komoda.ryosuke391@mail.kyutech.jp
A11	Lin TIAN	0000-0003-3841-3946	Institute of Materials Physics, Georg-August-University of Göttingen	Friedrich-Hund-Platz 1, 37077 Göttingen, Germany ltian@phys.uni-goettingen.de
A12	Juan SHANG	0000-0002-3234-5199	International Institute for Carbon-Neutral Energy Research (WPI-I2CNER), Kyushu University and Center for Energy Systems Design (CESD), International Institute for Carbon-Neutral Energy Research (WPI-I2CNER), Kyushu University	744 Motooka, Nishi-ku, Fukuoka, Fukuoka, 819-0395, Japan shang.juan.061@m.kyushu-u.ac.jp

Synopsis:

The objective of this study is to enhance the understanding of the mechanisms responsible for the reduced creep life in the presence of hydrogen, with the goal of ensuring the safety of advanced high-temperature hydrogen technologies. The material used in this study was pure iron, which, due to its simple chemical composition and single-phase microstructure, is a model system for examining the role of hydrogen in accelerated creep deformation.

Creep tests were conducted in hydrogen and argon gases at 873 K, with an absolute gas pressure of 0.12 MPa for both gases. The results showed that the creep strain rate in hydrogen gas was significantly accelerated, leading to a substantial reduction in creep life. The fracture surfaces and profiles exhibited dimple and double cup features, which were remarkably similar regardless of the test environment and applied stress.

Analysis of the secondary ~~steady-state~~ creep deformation indicated that the role of hydrogen was to reduce the creep activation energy. One possible mechanism for hydrogen's acceleration of creep deformation is enhanced dislocation climb, mediated by an increased vacancy density resulting from a reduction in vacancy formation energy due to hydrogen. In addition, it was found that decarburization during creep testing has a significant effect on reducing creep life. Importantly, the creep strain rate of pre-decarburized specimens was found to be higher in hydrogen than in argon, indicating the presence of a unique hydrogen effect that accelerates creep deformation.

Keywords:

Creep, Iron, Hydrogen, Decarburization, Dislocation climb

1. Introduction

There is significant potential for rapid advancements in high-temperature hydrogen technologies. Table 1 presents the technologies that utilize high-temperature hydrogen and are currently under research and development, along with their respective temperature ranges. As shown in the table, high-temperature hydrogen is being explored for various applications, including electricity generation, hydrogen production, fuel synthesis, power generation as an internal combustion engine, industrial processes, and heat and steam generation, all aimed at advancing the energy transition with carbon neutrality. With this ongoing research and development efforts, the demand for material strength tests in high-temperature hydrogen environments is increasing. Such tests require the use of relevant materials under appropriate mechanical and environmental conditions to investigate the deformation and failure mechanisms in high-temperature hydrogen environment.

High-temperature hydrogen can be a highly aggressive environment for structural materials. High-temperature hydrogen attack (HTHA) is the most well-known form of material damage that occurs in hydrogen at elevated temperatures [9, 10]. Hydrogen that penetrates into the material reacts with carbon to form methane bubbles with extremely high gas pressure, primarily at grain boundaries. This chemical reaction results in decarburization, which lowers the material's strength and toughness. Due to the combination of ultra-high pressure within the methane bubbles and the reduced material strength, voids formed at the grain boundaries lead to cracking, ultimately resulting in catastrophic failure of the structure. This mechanism was understood long ago, but in recent years, it has been further elucidated through microstructural observations using advanced microscopy techniques [11]. Additionally, modeling of void growth has been refined to accurately account for the interaction between dislocation creep and grain boundary diffusion [12]. This modeling has evolved to enable the development of Nelson-type curves [13], which account for the material microstructure, the deformation and failure mechanism, the applied structural stresses, and have the potential to eventually replace the classical Nelson empirical design approach [14].

Several studies have investigated the effects of hydrogen on creep, an important strength characteristic for structural components used at high temperatures. Yokogawa et al. observed a reduction in creep life during their creep experiments conducted in 9.9 MPa hydrogen at 773 K using pure iron [15]. They examined the mechanism responsible for the reduced creep life in hydrogen based on the transition of fracture mode from transgranular in argon (Ar) to intergranular in hydrogen (H2) and conducted detailed fracture surface analyses. Yokogawa et al. concluded that HTHA was responsible for the reduction in creep life. Specifically, they identified fine dimples on intergranular fracture surfaces.

McCoy and Douglas [16], McCoy [17], Schuster et al. [18], He et al. [19], Paraventi et al. [20], and Takazaki et al. [21] also reported reductions in creep life due to hydrogen. Takazaki et al. briefly reviewed these studies in his paper. In these works, various potential degradation mechanisms were examined, including the effect of hydrogen on dynamic precipitation of carbides [19], hydrogen-enhanced diffusivity of alloy elements, interactions between interstitial hydrogen and dislocations [17, 20], hydrogen-lowered surface energy [19], and enhanced dislocation climb mediated by increased vacancy density due to hydrogen [21], in addition to HTHA [15].

Takazaki et al. carried out creep test of SUS304 at 873 K under atmospheric pressure hydrogen and reported a significant increase in the creep strain rate in hydrogen compared to argon, leading to a substantial reduction in creep life [21]. They also found that the elongation at creep rupture and the reduction of area were larger in hydrogen than in argon. The fracture surface in argon transitioned from a dimple morphology to intergranular cracking at low applied stresses with a concomitant increase of the creep life. A similar transition occurred in hydrogen, however, hydrogen delayed this transition. In contrast to room- and low-temperature hydrogen embrittlement, where ductility loss is the most significant manifestation of hydrogen's effect and the fracture surface undergoes characteristic changes, the features observed in high-temperature

hydrogen creep exhibit the opposite trend [21]. Regarding the mechanism by which hydrogen accelerates creep strain rate, they proposed enhanced dislocation climb mediated by an increased vacancy concentration. This was concluded from the comparison of the experimentally measured creep strain rates with those predicted by the power-law equation for creep; hydrogen-induced reduction of the vacancy formation energy aligns the two sets of results. Additionally, based on further verification experiments, Takazaki et al. confirmed that the effect of HTHA, carbide formation and HELP were minor under their experimental conditions. Thus, they concluded that the most colorable role of hydrogen was to enhance dislocation climb through an increased vacancy population.

More recently, Motoyama et al. [22] conducted creep tests on~~f~~ SUS304 at 873, 973, and 1073 K under atmospheric pressure hydrogen and reported that hydrogen accelerated creep strain rate of SUS304 at 873 K and 973 K, resulting in reduction in creep life, whereas~~but~~ no~~t~~ such effect was observed at 1073 K. They suggested~~pointed out~~ that, if ~~the mechanism of~~ enhanced dislocation climb due to an increase vacancy population ~~through an increased vacancy population~~ is operative, the relative contribution of hydrogen-induced vacancies may diminish at higher temperatures~~,~~ because~~since~~ the ~~thermal~~ equilibrium vacancy concentration of thermally generated vacancies increases with temperature. ~~It should be~~ They also noted that ~~they also pointed out that~~ dynamic recrystallization was considered to dominate creep deformation at 1073 K, in contrast to the ~~defroamtion~~deformation behavior ~~results~~ observed at 873 ~~K~~ and 973 K, which may~~and this may have~~ have suppressed the contribution of hydrogen to plastic deformation.

Harris and Van Wanderham investigated properties of metallic materials, including creep properties, in high-pressure hydrogen at elevated temperatures [~~22~~23]. The effects of hydrogen varied depending on the material and testing conditions. They categorized the tested materials into four groups based on the degree of degradation caused by the hydrogen environment: extremely degraded (ED), severely degraded (SD), degraded (D), and negligibly degraded (ND). In their

creep rupture experiments, Inconel 718 and Inconel 625 were classified as SD. WASPALOY, IN-100, MAR M-200DS, A-28G, and Titanium 6-4 were classified as D. Astroloy, AISI 347, and Haynes 188 were classified as ND. However, the specific mechanisms underlying the varying degrees of degradation across different materials remained unclear.

As demonstrated in the above studies, several mechanisms have been proposed to explain the degradation of creep properties caused by hydrogen. However, definitive conclusions have yet to be reached. Therefore, this study aims to deepen the understanding of the mechanisms responsible for reduced creep life in hydrogen. To do this, the study is conducted in pure iron as the material whose single-phase microstructure offers an easy pathway to the interpretation of the results.

2. Experimental procedures

The test material used was JIS SUY-1 industrial pure iron. Although this material is not typically employed in structural applications for advanced high-temperature hydrogen technologies, its simple chemical composition and stable single-phase structure—not necessary to consider precipitation and phase transformations during high-temperature exposure—make it advantageous for investigating the mechanisms by which hydrogen influences creep deformation. Table 2 presents the chemical composition of the SUY-1. As a commercially available pure iron, it contains small amounts of carbon and other elements.

In this study, two different batches of pure iron, labeled as Lot 1 and Lot 2, were used in the creep tests. Lot 1 was used in its as-received condition to investigate the effect of hydrogen on creep properties. Lot 2 was used to study the role of decarburization in the reduction of creep life under hydrogen exposure. For this purpose, the carbon content in Lot 2 batches was adjusted through hydrogen heat treatment. Specimens were initially annealed in vacuum at 1273 K for 2 hours, followed by decarburization in hydrogen gas at 1073 K for specific durations to achieve the

desired carbon contents.

The microstructure of both batches of materials was nearly equiaxed, as shown in Fig. 1. The average grain size of Lot 1 was approximately 40 μm, whereas for batches in Lot 2, it ranged from 121 to 135 μm, slightly increasing as the duration of the hydrogen heat treatment increased. The carbon content of materials in Lot 2, measured by the infrared adsorption method after combustion, decreased significantly with increasing hydrogen heat treatment duration. Vickers hardness of Lot 1 was HV1 150. On the other hand, Vickers hardness of Lot 2 was HV1 73 after annealing and before hydrogen heat treatment, and ~~it reduced after the treatment, for example,~~decreased to HV1 59 after 27 hours of hydrogen heat treatment. Details of the microstructures, their relation to the heat treatments, the carbon content and Vickers hardness are summarized in Fig. 1. It should be noted that both Lot 1 and Lot 2 were commercially available pure iron obtained at different times, and that they differed in their initial chemical composition, grain size and hardness values.

Fig. 2 shows the shape and dimensions of the creep specimens. Round-bar specimens with a 30-mm gauge length were used. The specimen diameter was 4 mm for Lot 1 and 6 mm for Lot 2. The reason for using different specimen diameters for Lot 1 and Lot 2 was that the material strength of Lot 2 was expected to be lower than that of Lot 1, and we aimed to precisely control the applied stress. The specimen surface was polished by buffing to facilitate postmortem surface examination. Creep tests were conducted in hydrogen and argon gases at 873 K under an absolute pressure of 0.12 MPa. The purities of the supplied hydrogen and argon gases were 99.9999%. The main impurities in the gases were oxygen (< 0.1 volume ppm), carbon monoxide (< 0.1 volume ppm), carbon dioxide (< 0.1 volume ppm), and hydrocarbons (< 0.1 volume ppm). The water content was less than 0.5 volume ppm, with a corresponding dew point of 193 K.

Figure 3 shows the creep testing machine and a schematic illustration of the structure around the

hydrogen gas chamber. The testing machine was developed by the authors with technical support from PRETECH Co., Ltd. and financial support from the JSPS Grant-in-Aid for Scientific Research (B). Basically, the apparatus is a tensile creep testing machine equipped with a hydrogen gas chamber and a heating system.

The load was applied through a system in which the rotation of a servomotor was converted into axial linear motion by a ball screw and a linear slider. This mechanism enables precise maintenance of a constant applied load. During creep tests, the load was measured using a load cell attached to the bottom of the loading shaft, and the servomotor displacement was controlled to maintain the target load.

To maintain the purity of hydrogen gas during long-term creep tests, which sometimes exceeded 1,000 h in duration, the furnace was installed outside the gas chamber. Although this configuration results in lower heating efficiency, it ensures a clean gas environment. Bellows were installed at the lower part of the gas chamber and deformed with the applied displacement. This design eliminates the need for a sliding seal and consequently reduces the risk of hydrogen gas leakage.

The specimen temperature was monitored using a K-type thermocouple placed in contact with the specimen surface. The thermocouple was kept in contact with the midpoint of the specimen gauge length by its own spring action, and the contact was visually confirmed through an observation window of the gas chamber. During the creep tests, the temperature was maintained at 873 K within ±1 K. Although a single thermocouple was used during the tests, the temperature distribution along the specimen gauge length had been confirmed using multiple thermocouples prior to the creep tests.

In this study, the crosshead displacement was used as a proxy for specimen deformation instead of direct elongation measurements, because direct elongation measurements during creep test in high-temperature hydrogen gas require specialized equipment. Although the crosshead displacement includes elastic elongation of the testing machine components, such as the loading shaft and jigs, these contributions remain constant under the applied constant load. Therefore,

during creep deformation, the time-dependent change in crosshead displacement corresponds directly to the elongation of the specimen.

It was confirmed that the average difference between the creep elongation estimated from the crosshead displacement and that measured from gauge marks on the ruptured specimens was within approximately 1%, with a standard deviation of 5%.

To evaluate strain from the crosshead displacement instead of the elongation measured between gauge marks, the corrected reference length defined in JIS Z 2271, which accounts for deformation in the specimen shoulders, was adopted. In accordance with JIS Z 2271, the reference length was determined to be 32.7 mm for the specimens from Lot 1 and 32.4 mm for those from Lot 2.

As demonstrated experimentally by Nagao et al. [~~23~~24] hydrogen uptake in materials occurs easily at elevated temperatures, even when the surface is covered by an oxide layer. In this work, a uniform hydrogen concentration across the specimen diameter was the case. The hydrogen concentration in the specimen at 873 K and 0.12 MPa H_2 gas pressure was estimated to be 0.70 mass ppm with reference to Hirth's paper [~~24~~25]. The estimated time required to reach saturation was 1 minute for the 4 mm diameter specimen and 2 minutes for the 6 mm diameter specimen, based on the hydrogen diffusion coefficient in iron reported by Hirth [~~24~~25].

The hydrogen and argon gas environments were established after baking the gas chamber at 873 K under vacuum, following four cycles of vacuuming and purging with 99.9999% nitrogen gas. Prior to the start of the creep test in hydrogen, the specimens were soaked in the testing environment without a load for 2 hours to achieve uniform hydrogen distribution across the diameter. During the creep test, hydrogen penetrated not only the specimen but also the gas chamber wall. As a result, hydrogen gradually escaped from the gas chamber, causing a reduction in hydrogen gas pressure. To maintain the hydrogen gas pressure during the test, hydrogen was continuously supplied at a constant flow rate (100 ml/min). This flow rate was sufficient to

maintain a stable hydrogen pressure of 0.12 MPa throughout the test. For the creep tests in argon gas, there was no need to consider argon penetration into the specimen or chamber wall. However, the same procedure was applied to ensure consistent thermal history for the specimen and to maintain gas purity during the test.

3. Results and discussions

3. 1 Tensile test

Prior to creep testing, tensile tests were conducted at 293 K and 873 K in argon to determine the conditions for creep testing. The same specimen geometry used for the creep tests was utilized for these initial tests. The strain rate was set to 10−3 /s. Fig. 4 shows the stress-strain curves at both temperatures. It was observed that the SUY-1 industrial pure iron undergoes significant dynamic recovery, evidenced by the absence of work hardening after yielding, during the tensile test at 873 K. Consequently, the 0.2% proof strength and ultimate tensile strength were identical. This result suggests that the dislocations can climb as well as glide so that dislocation rearrangement and pair annihilation proceed quickly [25,26].

Table 3 summarizes the mechanical properties of the SUY-1 from Lot 1. The elongation at 873 K was significantly reduced compared to that at 293 K. This reduction is caused by the absence of work hardening. As indicated by the reduction of area, ductility actually increased. The absence of work hardening shortened the period of uniform elongation, resulting in the early onset of necking. Fig. 5 shows the fracture profiles and fracture surfaces of the tensile specimens. The fracture profiles exhibited a double-cup fracture, while the fracture surfaces displayed dimples at both temperatures.

3. 2 Reduction of creep life in hydrogen

Figure 6 shows the creep curves of the SUY-1 industrial pure iron. In this figure, in order to

clearly differentiate datasets with substantially different lifetimes, the results are shown in two separate graphs based on the lifetime range. The creep tests were performed under applied stresses of 33, 40, 50, and 60 MPa, which are significantly lower than the 0.2% proof strength at 873 K. As shown in the graph, the creep strain rate in the secondary creep ~~steady-state~~ region was markedly accelerated in hydrogen compared to argon, resulting in a significant reduction of creep life. The result that the creep life in hydrogen was reduced was similar to the result that Yokogawa et al. reached in their creep experiment with a commercial pure iron, conducted at 9.9 MPa hydrogen and 773 K [15]. It should be noted that the hydrogen gas pressure in our creep test, 0.12 MPa, was considerably lower than that in Yokogawa's experiment.

Given the experimental error of 1% with a 5% standard deviation in the measurement of elongation, we may state that the experimental results of Fig. 6 do not point to any definitive effect of stress or hydrogen on the creep ductility, except under stress 40 MPa. On the other hand, the experimental results of Takazaki et al. with SUS304 [21] show increased creep elongation in hydrogen. The lack of hydrogen or stress effect on creep elongation in our results along with the fact that the 98% reduction of area at rupture is the same in both hydrogen and argon is in contrast to hydrogen embrittlement at room and lower temperatures, at which ductility loss is a most significant manifestation of hydrogen embrittlement. Interestingly, Yokogawa et al. [15] observed in their experiments with pure iron that HTHA during creep testing significantly reduces elongation at creep rupture. This discrepancy in creep ductility in hydrogen between the two experiments using similar material is due to the operation of different mechanisms, depending on the hydrogen pressure and temperature. Specifically, Yokogawa et al. observed intergranular fracture surfaces, and proposed HTHA as the primary mechanism of failure, whereas we observed significant necking and dimple fracture surfaces and argue for enhanced dislocation climb mediated by hydrogen-induced vacancy formation, which will be discussed later. It should be also noted that Yokogawa et al. conducted creep tests under 9.9 MPa of high-pressure hydrogen at 773 K, whereas

we performed the creep tests under atmospheric hydrogen pressure at 873 K. Since the Nelson curve for pure iron is unavailable, we used the Nelson curve for carbon steel [26,27] instead. Yokogawa's hydrogen pressure and temperature were in the unsafe operation regime based on the Nelson curve for carbon steel, whereas our hydrogen pressure and temperature fall within the safe operation region.

Figure 7 shows the stress vs. creep rupture time curves of the SUY-1. Across the entire stress range over which the creep tests were carried out, the rupture time of specimens in hydrogen was shorter than that in argon. To ensure consistency, a second set of creep experiments was performed on Lot 1 specimens under 40 MPa applied stress. As demonstrated, the reduction in the creep life in hydrogen gas is significantly larger than the difference between the creep rupture times from the two experiments in argon or hydrogen under 40 MPa stress.

In Fig. 7, the creep lives of Lot 2 in both hydrogen and argon are substantially shorter than those of Lot 1, although both lots were the same JIS SUY-1 grade. The initial chemical composition, grain size, and hardness differed between Lot 1 and Lot 2. In addition, Lot 1 was used in the as-received condition, whereas Lot 2 was used after annealing and hydrogen heat treatment. As shown in Fig. 1, the hydrogen heat treatment resulted in changes in grain size and hardness. Therefore, the difference in creep life between Lot 1 and Lot 2 may be associated with differences in their material properties, including chemical composition, grain size, and hardness. However, clarifying the effects of these factors, including the effect of trace amounts of carbon on the creep deformation behavior of pure iron, would require considerable effort. We therefore consider this an important subject for future study.

It is important to understand at which stage of creep deformation the effects of hydrogen set in, as this is key for discussing the underlying mechanisms. Figure 8 shows the normalized creep curves, where the elapsed time for each creep test is normalized by the rupture life of each

specimen, for the tests conducted under applied stresses of 40 and 50 MPa. As can be seen the creep curves in hydrogen almost coincide with those in argon. The key insight from this graph is that hydrogen did not affect the deformation behavior during secondary and tertiary creep, nor the onset of tertiary creep. Therefore, one can argue that the reduced creep life in hydrogen was primarily due to the acceleration of the creep strain rate in the secondary ~~steady-state~~ creep regime. In other words, the reduction of the creep life observed in hydrogen is not caused by time-dependent microstructural changes, such as the formation of voids at grain boundaries.

Figure 9 shows the relationship between the rupture life and the minimum creep strain rate. Notably, the plots representing the results in hydrogen and those in argon lie along the same line. The fact that the creep life in both hydrogen and argon lie on a single line, the Monkman-Grant relation, indicates that the creep rupture life of the SUY-1 is governed solely by the minimum creep strain rate, independent of the testing environment. It should be noted that Yokogawa et al. [15] reported a shift in the Monkman–Grant line between argon and hydrogen environments in their experiments on pure iron and attributed this shift to high-temperature hydrogen attack (HTHA) as the underlying mechanism responsible for the reduced creep life in hydrogen.

After the creep tests in hydrogen and argon, the fracture profiles and fracture surfaces were examined, as shown in Fig. 10. In both environments, a double-cup fracture morphology was evident, reflecting significant necking. The reduction of area was nearly identical for both environments, while the elongation at creep rupture in hydrogen was greater than that in argon, as shown in Fig. 6. Dimples were observed on the fracture surfaces in both environments, with similar shapes and sizes, regardless of the testing atmosphere. As mentioned earlier, the accelerated creep strain rate in the ~~steady-state~~ secondary creep region is considered to be the primary contributor to the reduced creep life in H_2. Therefore, direct conclusions about the role of hydrogen in the reduced creep life cannot be drawn solely from the examination of the fracture surface, which

formed through significant local deformation during the tertiary creep stage. Nevertheless, the similarity of the fracture profiles and fracture surfaces in hydrogen and argon is noteworthy, and it does not support the assumption that a distinct fracture mechanism, such as the promotion of intergranular fracture, was active in hydrogen.

Figure 11 shows inverse pole figure (IPF) maps of the longitudinal cross sections of fractured specimens tested under an applied stress of 50 MPa in hydrogen and argon atmospheres. The black lines separating the grains indicate high-angle grain boundaries with misorientation angles greater than 15°. Beneath the fracture surface, in the necked region, the grains were refined compared with those in the original material in both hydrogen and argon environments. With regard to the grain morphology, relatively large grains were elongated along the tensile axis, whereas smaller grains tended to be more equiaxed. This microstructural feature suggests that dynamic recrystallization occurred during severe deformation in the necking region, leading to the formation of fine, equiaxed grains.

In contrast, no significant recrystallization was observed at a location approximately 5 mm underneath the fracture surface. This is likely because the local deformation and strain rate at this position were insufficient to trigger dynamic recrystallization. Therefore, recrystallization occurred only in the region that experienced pronounced necking during the tertiary creep stage. In both the recrystallized and non-recrystallized regions, no notable differences in microstructural evolution were observed between the hydrogen and argon environments, which is consistent with the fracture surface observations.

Vickers hardness was also measured at locations corresponding to the IPF maps, and the measured values are shown in the figure captions. The hardness tended to be slightly higher near the fracture surface than at the location 5 mm below the fracture surface in both hydrogen and argon. This increase may be associated with the grain refinement due to dynamic recrystallization

in the necked region and an increase in dislocation density due to significant plastic deformation in this region. However, the hardness values were comparable between the hydrogen and argon environments, which is consistent with the absence of significant differences in the IPF maps.

As shown in Fig. 1, the hardness of Lot 1 before creep testing was HV1 150. After the creep test, the hardness decreased to HV1 90 - 94 near the fracture surface and HV1 81-83 at the location 5 mm below the fracture surface. This significant reduction in hardness may be associated with dynamic recovery.

Figure 12 shows the creep deformation mechanism map [27,28] of Frost and Ashby for iron, with the experimental data from this study superimposed. In this diagram, the effective stress σ_s was calculated as $\sigma_s = \sigma/\sqrt{3}$, where σ is the applied tensile creep stress. The shear modulus μ of iron at 873 K is 45 GPa according to Frost and Ashby [27,28]. Fig. 12 indicates that our experimental data fall in the power-law creep region.

Figure 13 shows the minimum creep strain rate of Lot 1 and Lot 2-3 as a function of the applied stress. The minimum creep strain rate was increased in hydrogen across the entire stress range for both specimens. The minimum creep strain rate in the power-law creep region can be expressed by the following equation

$$\dot{\varepsilon} = A\left(\frac{\sigma}{E}\right)^n \exp\left(-\frac{Q_c}{RT}\right), \quad (1)$$

where $\dot{\varepsilon}$ is the minimum creep strain rate, A is a material constant serving as reference strain rate, σ is the applied stress, E is Young's modulus, n the stress exponent, Q_c the creep activation energy, R the gas constant, and T the absolute temperature. The slopes of the lines interpolating the data provide the stress exponent n, which is 5.6 ± 1.1 in hydrogen and 6.8 ± 0.2 in argon for Lot 1, and 6.0 ± 0.5 in hydrogen and 6.0 ± 0.2 in argon for Lot 2-3. The stress exponents obtained in hydrogen and argon were slightly different for Lot 1, whereas they were in

good agreement for Lot 2-3. In addition, the standard deviation of the stress exponent in hydrogen for Lot 1 was significantly larger than those under the other conditions. These results may be related to progressive decarburization during creep testing in hydrogen for Lot 1. In contrast, the Lot 2-3 specimens were decarburized prior to the creep tests, and no significant decarburization occurred during the creep tests. The decarburization that occurred during the creep tests is discussed later.~~-~~

Therefore, the discussion on the creep deformation mechanism hereafter is based on the stress exponents obtained for Lot 2-3. The stress exponents obtained in this study ~~The minimum creep strain rate data in hydrogen showed relatively larger scatter; however, all values fall within a factor of two of the scatter range. These values~~ are consistent with those reported in previous studies where creep tests were conducted in the power-law creep region for pure iron. For instance, Ishida et al. reported a value of 6.9 ~~28~~29), while Watanabe et al. reported 4.5 ~~29~~30). Based on these results and the fact that our testing conditions fall within the power-law creep region in Frost and Ashby's creep deformation mechanism map, we can conclude that the creep deformation mechanism active in both hydrogen and argon in this study is dislocation creep described by a power law relationship.

As mentioned earlier, there were no significant differences in the fracture profiles or fracture surfaces between hydrogen and argon. This observation further supports the assertion that the same creep deformation mechanism was active in both hydrogen and argon. Ongoing studies on creep-induced microstructural evolution in different gas environments support this conclusion, with detailed results to be reported elsewhere.

In equation (1), since the parameters A, E and R are constants, σ and T are experimental conditions that are fixed, and n obtained from Fig. 13 for hydrogen and argon with the two values being close, the only parameter that can be associated with accelerated creep strain rate, $\dot{\varepsilon}$ is the creep activation energy Q_c. For higher creep strain rates in hydrogen, Q_c in hydrogen should be

smaller than that in argon. Consequently, it can be deduced that the role of hydrogen in the accelerated creep deformation is the reduction of creep activation energy.

In this study, the creep activation energy was determined from the temperature dependence of the minimum creep strain rate at a constant modulus-compensated stress, σ/μ, over the temperature range of 773 ~ 873 K. Lot 2-3 was used for this experiment to exclude the effect of decarburization during creep testing, which may depend on temperature. The absence of decarburization in Lot 2-3 during creep testing was experimentally confirmed, as discussed later. Figure 14 shows the relationship between $ln\ \varepsilon$ and $1/T$. The creep activation energy can be expressed as:

$$Q_c = -R[\delta(ln\ \varepsilon)/\delta(1/T)]_{\sigma/\mu}$$

Therefore, the slopes of the fitted lines in Fig. 14 correspond to $-Q_c/R$. The creep activation energy obtained in this study was 227±12 kJ/mol in hydrogen and 244±14 kJ/mol in argon, suggesting that the creep activation energy may be lower in hydrogen.

The creep activation energy is generally comparable ~~almost equal~~ to the activation energy for self-diffusion in the power-law creep regime [30,31]. The creep activation energy in argon obtained in this study is consistent with the reported activation energies for self-diffusion in α-iron (240 - 300 kJ/mol[32]). This result is also consistent with the interpretation based on the stress exponent, which indicates that the creep deformation in this study occurs in the power-law creep regime.

The activation energy for self-diffusion can be expressed as the sum of the vacancy formation and vacancy migration energies [33,34]. In view of studies that report that hydrogen reduces the vacancy formation energy in α-iron [34,36,64], it can be stated that the reduced creep activation energy in hydrogen is the result of reduction of the vacancy formation energy. This reduction leads to higher vacancy concentration, thus providing increased opportunities for dislocation climb, which

414 is the dominant mechanism in the power-law creep regime. As a result, the creep strain rate
415 increases.
416
417 A similar mechanism was proposed by Takazaki et al. for SUS304 austenitic stainless steel [21]. It
418 is notable that independent experiments for BCC and FCC materials yield similar conclusions.
419 However, in both cases, the proposed mechanism remains hypothetical and plausible unless direct
420 evidence of hydrogen increasing vacancy concentration is confirmed. Further experiments and
421 examinations are required to reach a more definitive conclusion.
422
423 **3. 3 Effect of decarburization**
424 At elevated temperature, carbon at the specimen surface may react with hydrogen or other
425 gaseous impurities such as water vapor, which leads to surface decarburization. Consequently, a
426 carbon concentration gradient is formed, which drives the diffusion of carbon from the interior of
427 the specimen toward the surface during exposure to the testing environment, resulting in bulk
428 decarburization. The carbon content in the SUY-1 Lot 1 was 46 mass ppm, which is lower than the
429 carbon solubility limit of iron at 873 K according to Ohtani et al. [375]. As a result, carbon can
430 segregate at grain boundaries, resulting in local carbon contents exceeding 10 atom % when the
431 average carbon content is 46 mass ppm [386]. It was reported that carbon segregating at grain
432 boundaries increases the Hall-Petch coefficient leading to increased mechanical strength at room
433 temperature [379]. In this study, it may be possible that hydrogen enhances decarburization during
434 creep testing. Therefore, the effect of decarburization on the creep deformation of pure iron is
435 worth investigating.
436
437 In this study, the carbon content in an untested specimen and several creep-tested specimens was
438 measured using the infrared adsorption method. From each specimen, three samples, each weighing
439 1.0 g, were extracted and thus, three measurements were conducted for each specimen. Figure 14

15 shows the average carbon content and standard deviation from these measurements for the specimens subjected to creep at 60 and 33 MPa applied stress in hydrogen and argon environments. In both environments, the carbon content in the specimen significantly decreased compared to the original material, indicating decarburization during the creep tests.

With regard to decarburization in argon, since argon is inert, it may be caused by gas impurities such as water contained in argon. For the specimens tested at 33 MPa, the creep rupture time was 136 h in hydrogen and 811 h in argon. However, the carbon content in hydrogen was lower than that in argon which indicates that decarburization was promoted in hydrogen. On the other hand, there was no significant difference in the carbon content between the specimens that crept under 60 MPa in hydrogen and argon, although the carbon content decreased from that of the as received material, 46 wt ppm. Possibly, the time of exposure to testing environment was insufficient to cause a noticeable difference.

It is well-known that HTHA is a phenomenon that occurs in hydrogen at elevated temperatures and involves decarburization. Yokogawa et al. identified traces of HTHA during creep testing in H_2 on industrial pure iron, based on the observation of intergranular cracking on the fracture surface [15]. However, in our creep experiments at low hydrogen gas pressure, HTHA can be excluded as a mechanism responsible for the reduced creep life in H_2, and also because dimple fracture surfaces were observed in both hydrogen and argon. Moreover, since methane cannot diffuse out of the specimen, carbon remains in the material. As a result, any decrease in carbon content within the specimen cannot be detected using the infrared absorption method. Additionally, the environmental testing conditions in this study, including hydrogen gas pressure and temperature, were within the safe region specified by the Nelson diagram for carbon steels [26~~2~~27].

To study the effect of decarburization on creep life, decarburized specimens with carbon

contents of 9.9 ppm and 6.4 ppm were prepared, as described in Section 2. Figure ~~15~~ 16 shows the results of the creep test performed under 40 MPa stress in argon and hydrogen for the three levels of carbon content. As can be seen, the creep life in argon increases as the carbon content increases. This result clearly demonstrates that carbon, which may segregate at grain boundaries, enhances the creep resistance of pure iron. Regarding the mechanism underlying the enhanced creep deformation in the low-carbon material, the activation energy for vacancy formation, Q_c, in Eq. (1), has been reported to decrease with increasing carbon content [~~38~~40, ~~41~~39]. It should be noted here that Kabir et al. [~~41~~39] concluded that self-diffusivity in bcc Fe decreases with increasing carbon content, as the migration barriers of vacancy-carbon point-defect cluster are sufficiently high. This conclusion on iron self-diffusion was later corrected by Kresse et al. [~~4~~20] who demonstrated that iron self-diffusion is accelerated in the presence of dissolved carbon. Kresse et al. attributed this to an increased vacancy concentration due to the attractive interaction between vacancies and carbon atoms. According to Eq. (1), a decrease in vacancy formation energy would result in higher creep strain rates. However, our experimental results show that the strain rate decreases as the carbon content increases, which appears to be at odds with the implications of the work of Frost et al. [~~38~~40] and Kresse et al. [~~39~~42] that argue for decreasing vacancy formation energy with carbon. The pre-exponential factor A in Eq. (1) is generally considered a material constant. However, considering that our experimental results show that a reduction in the carbon content leads to an opposite effect on the creep strain rate to that dictated by the associated increase of Q_c, one may conclude that differences in carbon content cause the material to behave differently. Specifically, carbon atoms may reduce the value of A, possibly by lowering the formation energy of dislocations at grain boundaries or by reducing their mobility. Whether such a carbon-induced reduction in dislocation mobility persists at elevated temperatures remains unclear. However, it is clearly present at room temperature, as indicated by the yield strength overshoot observed in Fig. 4. With respect to the effect of hydrogen, the creep life of the decarburized specimens was further reduced in hydrogen.

Figure ~~16~~ 17 shows the measured carbon content of Lot 2 specimens before and after creep straining under 40 MPa. For the un-decarburized specimen, Lot 2-1 (no hydrogen treatment), the reduction of the carbon content after the creep test was significant (from 55 mass ppm to 18 mass ppm in hydrogen and 10 mass ppm in Ar), as the initial carbon content was sufficiently high. The remaining carbon content in the specimen tested in hydrogen was higher than that in argon, which appears inconsistent with the results shown in Fig. ~~14~~ 15 in which hydrogen is shown to promote higher decarburization. This discrepancy is attributed to the difference in creep life: 23.4 h in hydrogen vs 56.7 h in argon. The shorter exposure time for the specimen tested in hydrogen resulted in less decarburization. For the pre-decarburized specimens, the average carbon content before the creep test was 9.9 mass ppm after 9 h of hydrogen treatment of Lot 2-2 and 6.4 mass ppm after 27 h of Lot 2-3. Although these data appear to suggest that a longer hydrogen treatment further reduces the carbon content, the upper and lower bounds of the error bars are nearly identical. Therefore, when experimental variability is taken into account, the decarburization process can be regarded as having reached saturation within 9 h. With regard to the carbon content after the creep test, the value measured for the 27 h-treated specimen tested in argon was slightly higher than that tested in hydrogen; however, this difference is also considered to be within the range of measurement variability.

The key conclusion from Figure ~~16~~ 17 is that the reduction of the carbon content during the creep tests was minimal for the specimens that were pre-decarburized by heat treatment (9 h for Lot 2-2 and 27 h for Lot 2-3). As shown in Figure 1~~5~~6, the creep life of these specimens whose carbon content remained nearly constant during testing in hydrogen was significantly shorter than that in argon. These results clearly indicate that the reduction in creep life in hydrogen occurred independently of decarburization. These findings suggest that two distinct effects - decarburization and hydrogen - simultaneously contribute to the reduction of creep life during creep testing of pure iron in hydrogen. While decarburization reduces the creep life of pure iron, hydrogen separately reduces the creep life.

Lastly, Regarding the grain size effect, when comparing the creep lives of the un-decarburized Lot 2 (Fig. ~~16~~17) with those of Lot 1 (Fig. 6 (b)), the creep life of Lot 2 is shorter than that of Lot 1 in both hydrogen and argon environments under a stress of 40 MPa, despite its slightly higher carbon content (55 mass ppm vs 46 mass ppm). Creep strain rate is generally considered to show little dependence on grain size [~~27~~28]. However, in this study, differences in creep behavior were observed depending on the carbon content, which is thought to segregate at grain boundaries, suggesting that grain boundaries may play an important role in creep strength. Therefore, the coarser grain size of Lot 2 may have contributed to its shorter creep life.

4. Conclusion

Creep tests with SUY-1 industrial pure iron were conducted at 873 K in 0.12 MPa hydrogen and argon gases. The results are summarized as follows:

1. Hydrogen increased the minimum creep strain rate, leading to a significant reduction in creep life.
2. The normalized creep curves in hydrogen were found almost completely overlapping with those in argon. Additionally, the relationship between rupture life and minimum creep strain rate in hydrogen is the same as that in argon and linear. Furthermore, there was no significant difference in the morphology of the fracture surface between the specimens tested in argon and those in hydrogen. These results indicate that the primary role of hydrogen is to accelerate creep deformation without altering the intrinsic creep deformation mechanism.
3. Dislocation creep was activated in both hydrogen and argon environments, as shown by the calculation of the stress exponent and juxtaposition of experimental results on the Frost and Ashby creep deformation mechanism map for iron.
4. The creep activation energy determined from the temperature dependence of the minimum

creep strain rate was 227±12 kJ/mol in hydrogen and 244±14 kJ/mol in argon, suggesting that the creep activation energy may be lower in hydrogen than in argon. ~~Analysis of the minimum creep strain rates, based on the standard constitutive model for dislocation creep, suggests that hydrogen likely decreases the creep activation energy.~~ Consequently, we propose that hydrogen promotes dislocation climb through an increase in vacancy density due to the reduction of the vacancy formation energy by hydrogen.

5. Decarburization occurred during the creep tests in both hydrogen and argon environments, with hydrogen enhancing the decarburization process. However, no evidence of methane bubble formation was observed.

6. The creep life in argon decreased as the carbon content decreased, confirming that carbon improves creep strength of pure iron.

7. Decarburization during the creep tests contributed significantly to the shortening of the creep life in hydrogen. However, the creep life of the pre-decarburized specimens was further reduced in hydrogen, suggesting that hydrogen's unique effects- such as promotion of dislocation climb as we have proposed- contribute independently of decarburization to the reduction of creep life.

Statement for Conflict of Interest

The authors declare no conflicts of interest regarding this manuscript.

Acknowledgements

Part of this study was supported by the Research Fellowship for Young Scientists from the Japan Society for the Promotion of Science (JSPS), Grant Number 18J22540, and JSPS KAKENHI Grant Numbers 16H04237 and 20H00218. Additional support was provided by the contracted research funded under the JSPS JRP-LEAD with DFG program (Grant Number JPJSJRP 20221605), as well as by the Establishment of University Fellowships toward the Creation of Science and Technology

570 Innovation program (Grant Number JPMJFS2132) and JST SPRING, Japan (Grant Number
571 JPMJSP2136), both administered by the Japan Science and Technology Agency (JST). The authors
572 gratefully acknowledge the support of the International Institute for Carbon-Neutral Energy
573 Research (WPI-I2CNER) and its affiliated research institute, the Center for Energy Systems
574 Design.
575

576 **REFERENCES**

577 1) D. J. L. Brett, A. Atkinson and N. P. Brandon: *Chem. Soc. Rev.,* 37 (2008), 1568.
578 https://doi.org/10.1039/B612060C
579 2) S. E. Wolf, F. E. Winterhalder, V. Vibhu, L. G. J. de Haart, O. Guillon, R. A. Eichel and N. H.
580 Menzler: *J. Mater. Chem. A,* 11 (2023), 17977. https://doi.org/10.1039/D3TA02161K
581 3) Ministry of Economy, Trade and Industry (METI): Hydrogen gas turbine: toward realizing a
582 hydrogen society (in Japanese), Discussion on Gas Business in 2050: 2nd Meeting Materials,
583 2020.
584 https://www.meti.go.jp/shingikai/energy_environment/2050_gas_jigyo/pdf/002_07_00.pdf,
585 (accessed 2026-06-08).
586 4) H. Nickel, E. Bodmann and H. J. Seehafer: *Energy*, 16 (1991), 221.
587 https://doi.org/10.1016/0360-5442(91)90102-R
588 5) P. E. Miranda (ed.): Science and engineering of hydrogen-based energy technologies: hydrogen
589 production and practical applications in energy generation, Academic Press, (2018), ISBN
590 9780128142523
591 6) C. Gutiérrez-Antonio, F. I. Gómez-Castro, J. A. de Lira-Flores and S. Hernández: *Renew.*
592 *Sustain. Energy Rev.,* 79 (2017), 709. https://doi.org/10.1016/j.rser.2017.05.108
593 7) K. E. Lamb, M. D. Dolan and D. F. Dennedy: *Int. J. Hydrog. Energy,* 44 (2019), 3580.
594 https://doi.org/10.1016/j.ijhydene.2018.12.024
595 8) C. Kamijo, Y. Matsukura, H. Yokoyama, K. Sunahara, K. Kakiuchi, H. Sakaki, K. Nakano, Y.

596 Ujisawa and K. Nishioka: *ISIJ Int.,* 62 (2022), 2433.
597 https://doi.org/10.2355/isijinternational.ISIJINT-2022-099
598 9) A. A. Sagüés, B. O. Hall and H. Wiedersich: *Scr. Metall.,* 12 (1978), 319.
599 https://doi.org/10.1016/0036-9748(78)90121-7
600 10) P. G. Shewmon: *Mater. Sci. Tech.,* 1 (1985), 2. https://doi.org/10.1179/mst.1985.1.1.2
601 11) M. L. Martin, M. Dadfarnia, S. Orwig, D. Moore and P. Sofronis: *Acta Mater.*, 140 (2017),
602 300. https://doi.org/10.1016/j.actamat.2017.08.051
603 12) M. Dadfarnia, M. L. Martin, D. E. Moore, S. E. Orwig and P. Sofronis: *Int. J. Fract.*, 219
604 (2019), 1. https://doi.org/10.1007/s10704-019-00376-8
605 13) K. Vijayvargia, M. Dadfarnia, P. Sofronis, M. Kubota, A. Staykov, K. Wada, J. A. Pugh and T.
606 J. Eason: *Int. J. Fract*., 243 (2023), 203. https://doi.org/10.1007/s10704-023-00739-2
607 14) K. Vijayvargia, M. Dadfarnia, J. L. Bassani and P. Sofronis: *Int. J. Hydrog. Energy*, 136
608 (2025), 713. https://doi.org/10.1016/j.ijhydene.2024.05.456
609 15) K. Yokogawa, S. Fukuyama and K. Kudo: *J. Jpn. Inst. Met. Mater.*, 46 (1982), 1009.
610 https://doi.org/10.2320/jinstmet1952.46.10_1009
611 16) H. E. McCoy and D. A. Douglas Jr.: Effect of environment on the creep properties of type 304
612 stainless steel at elevated temperatures, Report No. ORNL-2972, Oak Ridge National
613 Laboratory, (1962). https://doi.org/10.2172/4782789
614 17) H. E. McCoy: Effects of hydrogen on the high-temperature flow and fracture characteristics of
615 metals, Report No. ORNL-3600, Oak Ridge National Laboratory, (1964).
616 https://doi.org/10.2172/4059624
617 18) G. B. A. Schuster, R. A. Yaske and C. J. Altstetter: *Metall. Trans. A,* 11 (1980), 1657.
618 https://doi.org/10.1007/BF02660520
619 19) J. He, G. Han, S. Fukuyama, K. Yokogawa and A. Kimura: *Acta Mater.,* 45 (1997), 3377.
620 https://doi.org/10.1016/S1359-6454(96)00400-4
621 20) D. J. Paraventi, T. M. Angeliu and G. S. Was: *Corrosion*, 58 (2002), 675.

https://doi.org/10.5006/1.3287697

21) D. Takazaki, T. Tsuchiyama, R. Komoda, M. Dadfarnia, B. P. Somerday, P. Sofronis and M. Kubota: *Corrosion*, 77 (2021), 256. https://doi.org/10.5006/3678

~~21)~~ K. Motoyama, K. Okumura, D. Kano, K. Wada and M. Kubota: Proceedings of the ASME 2026 Pressure Vessels and Piping Conference, PVP2026, ASME, New York, (2026), PVP2026-175087.

22)

~~22)~~23) J. A. Harris and M. C. Van Wanderham: Properties of materials in high pressure hydrogen at cryogenic, room, and elevated temperatures, PWA Report FR-5766, Pratt and Whitney Aircraft, West Palm Beach, FL, (1973). https://ntrs.nasa.gov/citations/19730023072, (accessed 2026-08-27).

~~23)~~24) A. Nagao, S. Takagi, N. Ishikawa and M. Kimura: Hydrogen uptake in steels exposed to high-pressure H_2 gas, International Hydrogen Conference (IHC 2016): Materials Performance in Hydrogen Environments, ed. by B. P. Somerday and P. Sofronis, ASME Press, (2017), 462. https://doi.org/10.1115/1.861387_ch52

~~24)~~25) J. P. Hirth: *Metall. Trans. A,* 11 (1980), 861. https://doi.org/10.1007/BF02654700

~~25)~~26) T. Suzuki, S. Takeuchi and H. Yoshinaga: Dislocation dynamics and plasticity (Vol. 12), Springer Science & Business Media, (2013). https://doi.org/10.1007/978-3-642-75774-7

~~26)~~27) API RP 941: 2016, Steels for hydrogen service at elevated temperatures and pressures in petroleum refineries and petrochemical plants.

~~27)~~28) H. J. Frost and M. F. Ashby: Deformation-mechanism maps: The plasticity and creep of metals and ceramics, Pergamon Press, Oxford, (1982). ISBN 0080293387.

~~28)~~29) Y. Ishida, C. Y. Cheng, J. E. Dorn: Creep mechanisms in alpha iron, Lawrence Berkeley National Laboratory, LBNL Report, UCRL-16416, (1965). https://escholarship.org/uc/item/724091hp

~~29)~~30) T. Watanabe and S. Karashima: *Trans. Jpn. Inst. Met.,* 11 (1970), 159.

https://doi.org/10.2320/matertrans1960.11.159

31) O. D. Sherby and A. K. Miller: *J. Eng. Mater. Technol.*, 101 (1979), 387. https://doi.org/10.1115/1.3443708

~~30)~~32) B. Zhang: *AIP Adv.*, 4 (2014), 017128. https://doi.org/10.1063/1.4863462

~~31)~~33) S. Takeuchi, H. Ino and E. Furubayashi: The physics of metallic materials (in Japanese), *Nikkan Kogyo Shimbunsha,* (1992). ISBN 9784526030857

~~32)~~34) Y. Tateyama and T. Ohno: *Phys. Rev. B,* 67 (2003), 174105. https://doi.org/10.1103/PhysRevB.67.174105

~~33)~~35) R. Matsumoto, N. Nishiguchi, S. Taketomi and N. Miyazaki: *J. Soc. Mater. Sci. Jpn.,* 63 (2014), 182. https://doi.org/10.2472/jsms.63.182

~~34)~~36) M. L. Fullarton, R. E. Voskoboinikov and S. C. Middleburgh: *J. Alloy. Compd.,* 587 (2014), 794. https://doi.org/10.1016/j.jallcom.2013.10.169

~~35)~~37) H. Ohtani, M. Hasebe and T. Nishizawa: *Trans. Iron Steel Inst. Jpn*., 24 (1984), 857. https://doi.org/10.2355/isijinternational1966.24.857

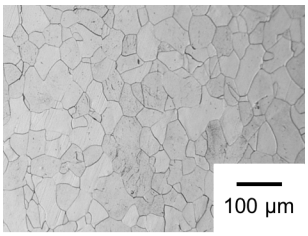
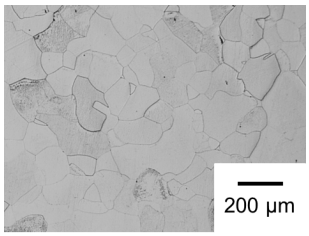
~~36)~~38) T. Tokunaga, Y. Motomura, H. Era, T. Tsuchiyama, K. Shobu, M. Hasebe and H. Ohtani: *Tetsu-to-Hagane*, 109 (2023), 158. https://doi.org/10.2355/tetsutohagane.TETSU-2022-081

~~37)~~39) S. Araki, D. Akama, T. Tsuchiyama, S. Takaki, T. Ohmura and J. Takahashi: *Tetsu-to-Hagane*, 103 (2017), 491. https://doi.org/10.2355/isijinternational.ISIJINT-2018-130

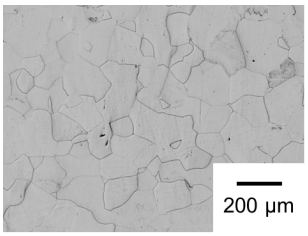
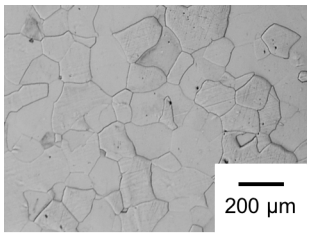
~~38)~~40) C. J. Först, J. Slycke, K. J. Van Vliet and S. Yip: *Phys. Rev. Lett.,* 96 (2006), 175501. https://doi.org/10.1103/PhysRevLett.96.175501

~~39)~~41) M. Kabir, T. T. Lau, X. Lin, S. Yip and K. J. Van Vliet: *Phys. Rev. B,* 82 (2010), 134112. https://doi.org/10.1103/PhysRevB.82.134112

~~40)~~42) T. Kresse, C. Borchers and R. Kirchheim: *Scr. Mater.,* 69 (2013), 690. https://doi.org/10.1016/j.scriptamat.2013.08.001

		
Time for Hydrogen heat treatment (hour)	Not applied (As received)	Not applied (As annealed)~~0~~
Carbon content (mass ppm)	45.7 ± 5.8	54.8 ± 6.1
Grain size (µ~~m~~m)	40	121
Vickers hardness (HV1)	150	73
	(a) Lot 1	(b) Lot 2-1

673

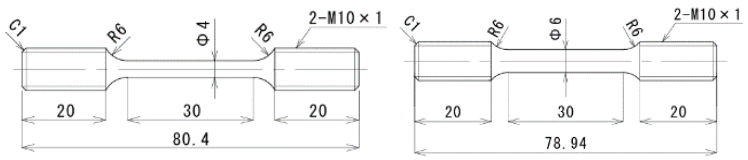
		
Time for Hydrogen heat treatment (hour)	9	27
Carbon content (mass ppm)	9.9 ± 1.5	6.4 ± 1.9
Grain size (µm)	123	135
Vickers hardness (HV1)	69	59
	(c) Lot 2-2	(d) Lot 2-3

674 Fig. 1. Microstructure, carbon content, grain size and Vickers hardness of the SUY-1 industrial

675 pure iron.

676

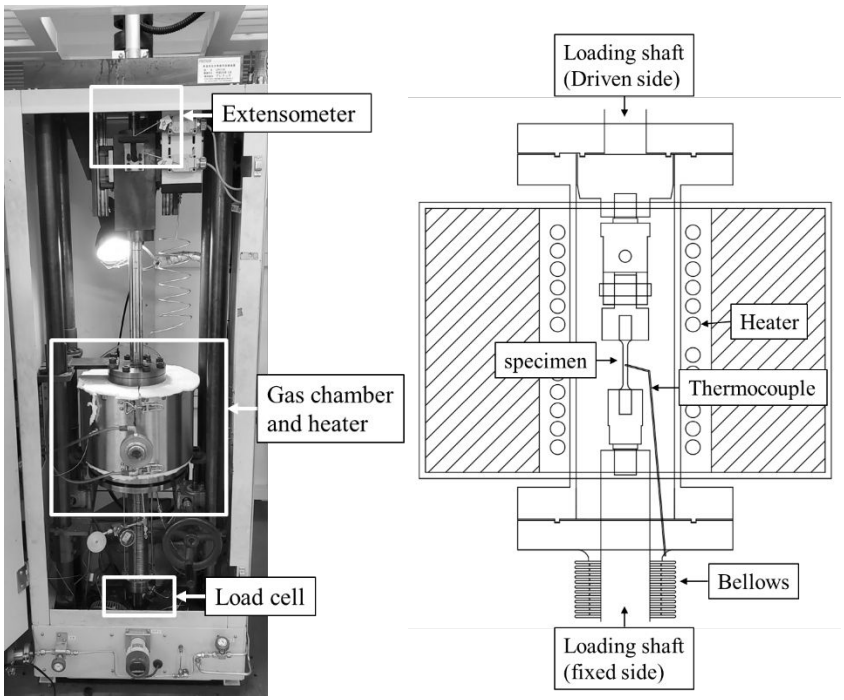
677



678 (a) For Lot 1 (b) For Lot 2

679 Fig. 2. Specimen drawings showing dimensions for (a) Lot 1 and (b) Lot 2.

680

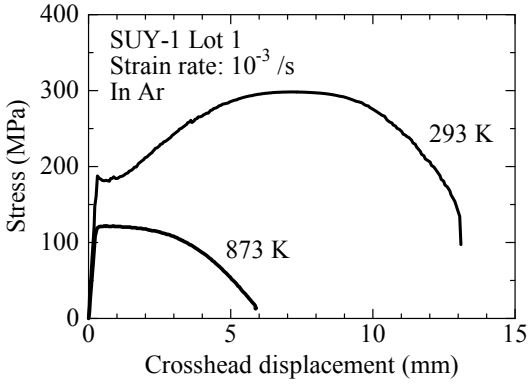


681

682 Fig. 3. (a) View of the creep testing machine and (b) Schematic of the structure around the gas

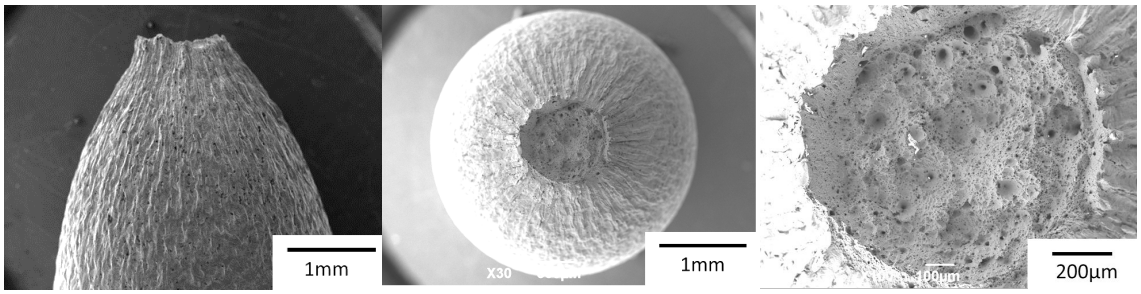
683 chamber.

684

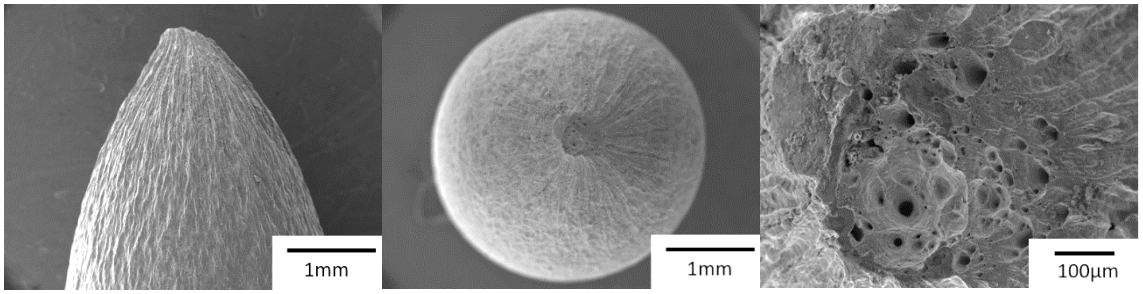


685

686 Fig. 4. Uniaxial tension tests with Lot 1 specimens at 298 and 873K.

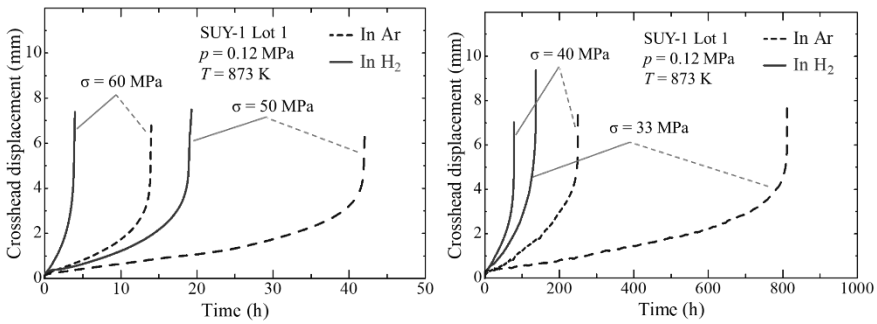


(a) 293 K



(b) 873 K

Fig. 5. Fracture profiles and fracture surfaces of tensile tests with Lot 1 specimens: a) at room temperature, b) at 873K.



(a) (b)

Fig. 6. Creep curves of the SUY-1 Lot 1 in hydrogen and argon under: (a) applied stress σ = 50 and 60 MPa, (b) applied stress σ = 33 and 40 MPa.

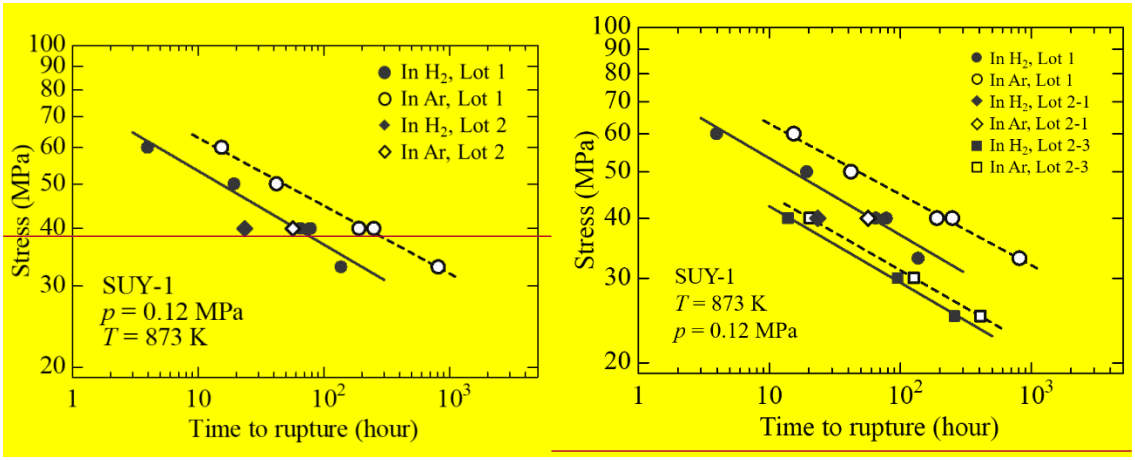
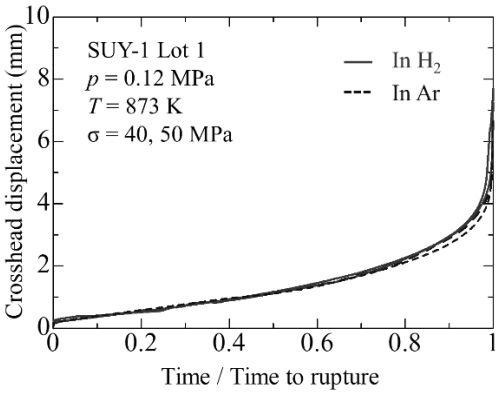


Fig. 7. Stress vs. rupture time curves of the SUY-1 Lot 1 and ~~un-decarburized~~ Lot 2 ~~at 40 MPa~~ in hydrogen and argon.

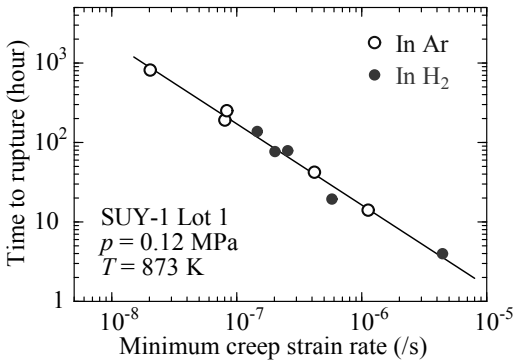


704

705 Fig. 8. Normalized creep curves of the SUY-1 Lot 1 in hydrogen and argon environment at stresses

706 40 and 50 MPa.

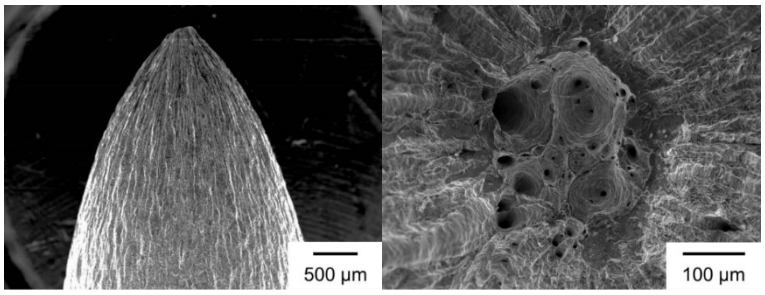
707



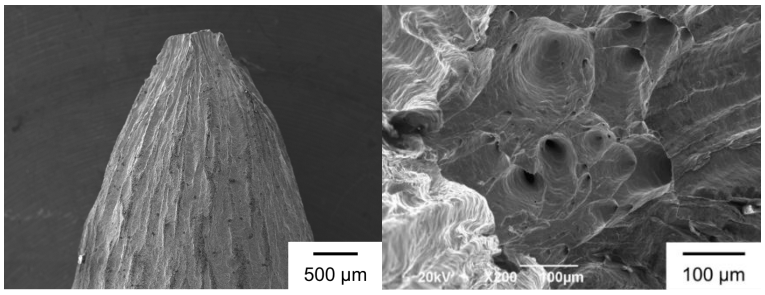
708

709 Fig. 9. Rupture life vs. minimum creep strain rate of the SUY-1 Lot 1.

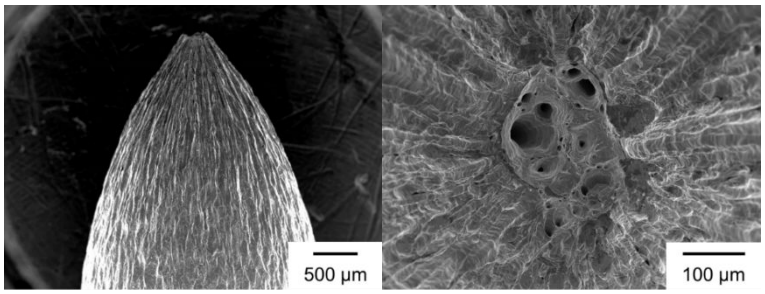
710



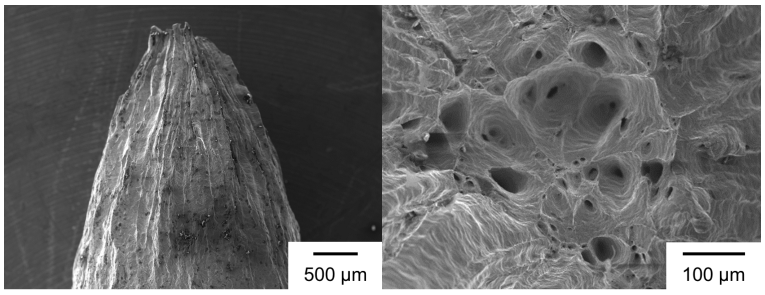
(a) In argon, σ = 60 MPa, t_r = 14.0 h



(b) In argon, σ = 33 MPa, t_r = 811 h



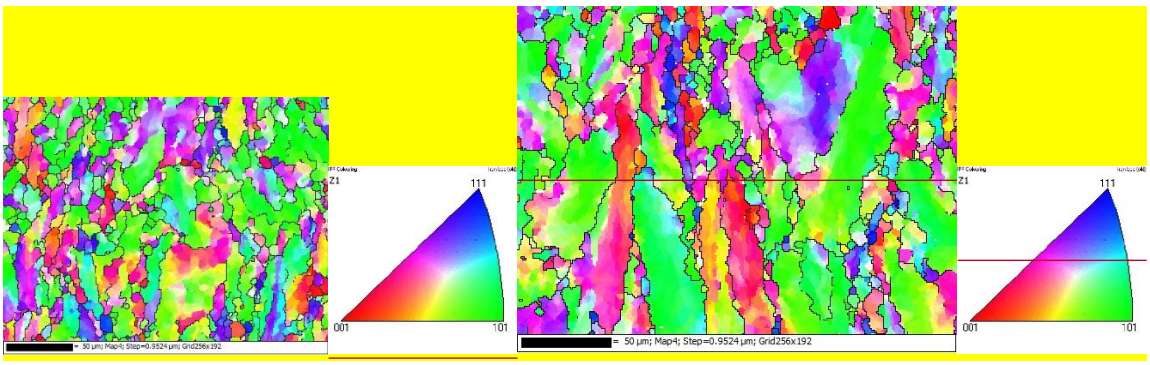
(c) In hydrogen, σ = 60 MPa, t_r = 4.0 h



(d) In hydrogen, σ = 33 MPa, t_r = 136 h

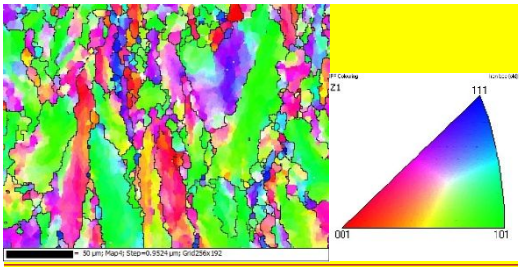
Fig. 10. Fracture profiles and fracture surfaces of Lot 1 specimen.

721



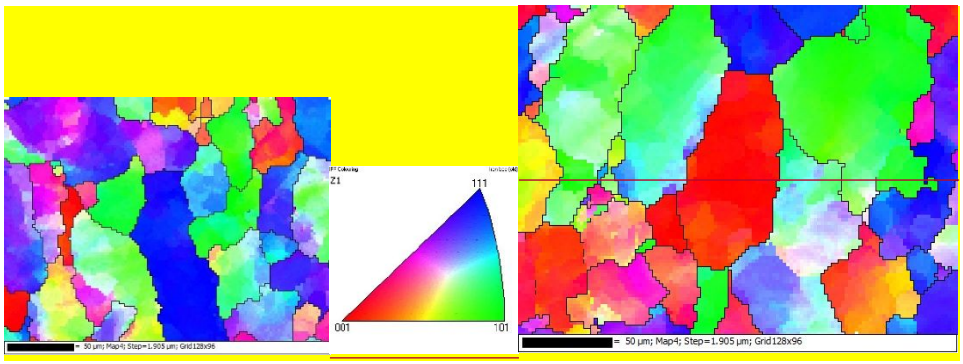
722

723 (a) Just below the fracture surface in H_2 (Vickers hardness: HV1 94).



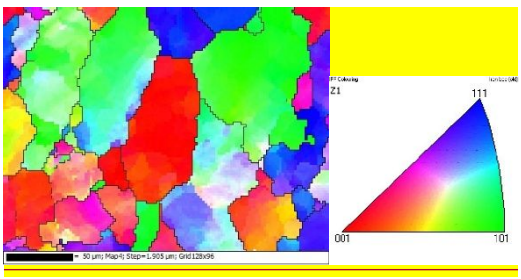
724

725 ~~(a)~~(b) ~~(b)~~ Just below the fracture surface in Ar (Vickers hardness: HV1 90).



726

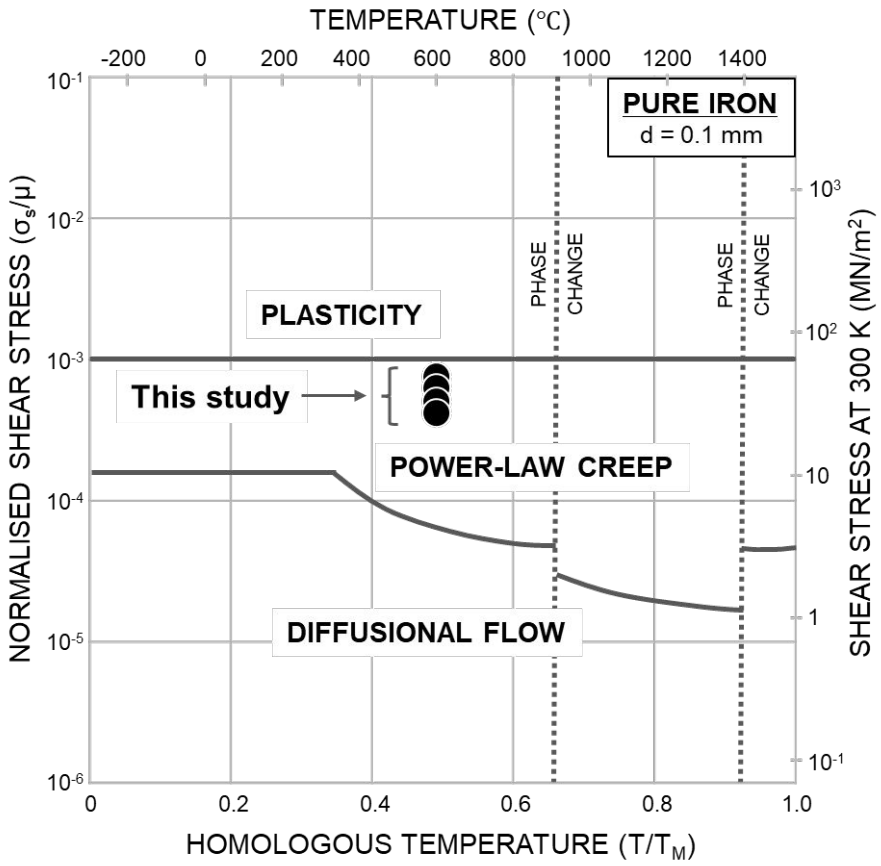
727 (c) ~~(c)~~ 5 mm underneath the fracture surface in H_2 (Vickers hardness: HV1 81).



728

729 (d) 5 mm underneath the fracture surface in Ar (Vickers hardness: HV1 83).

Fig. 11. Inverse pole figure (IPF) maps of longitudinal cross section of creep-fractured specimens of Lot 1 material tested under an applied stress of 50 MPa. (Rupture life in hydrogen: 19.3 h, rupture life in argon: 42.1 h.)

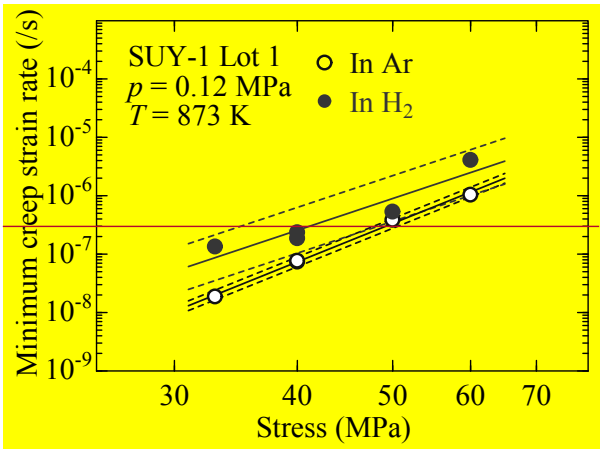


734

735 Fig. 12. Creep data superposed on the creep deformation mechanism map of Frost and Ashby [27] for

736 pure iron (redrawn by authors).

737



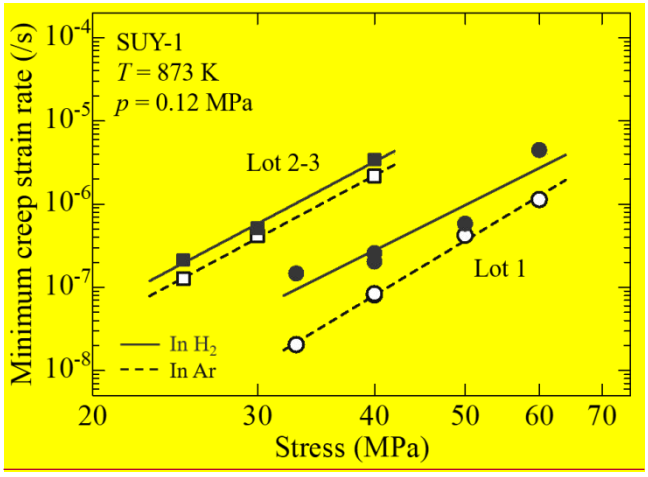
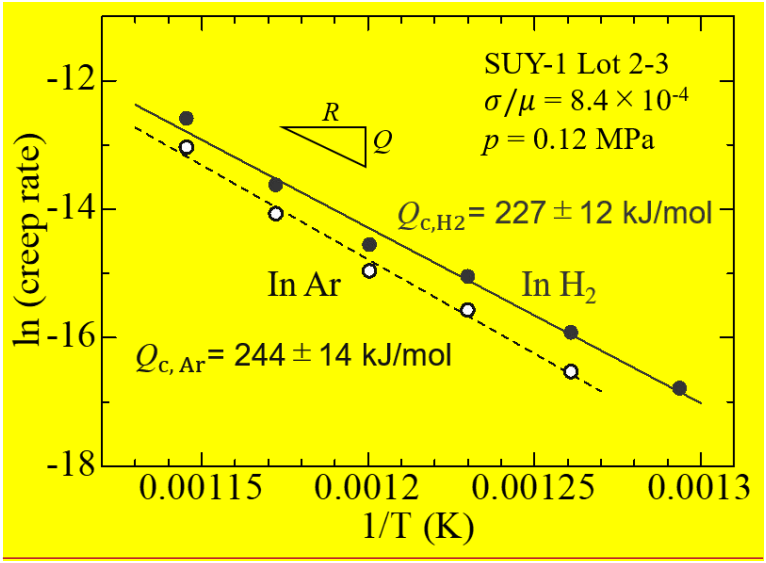


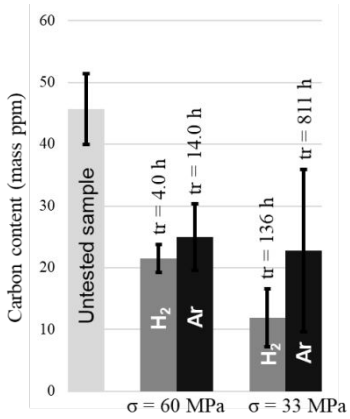
Fig. 13. Minimum creep strain rate vs. applied stress for SUY-1. The slope ~~in argon~~ is $n = 6.8 \pm 0.2$ in argon and ~~in hydrogen~~ $n = 5.6 \pm 1.1$ in hydrogen for Lot 1, and $n = 6.0 \pm 0.2$ in argon and $n = 6.0 \pm 0.5$ in hydrogen for Lot 2-3.



744

745 Fig. 14. Creep test results for determining creep activation energies.

746

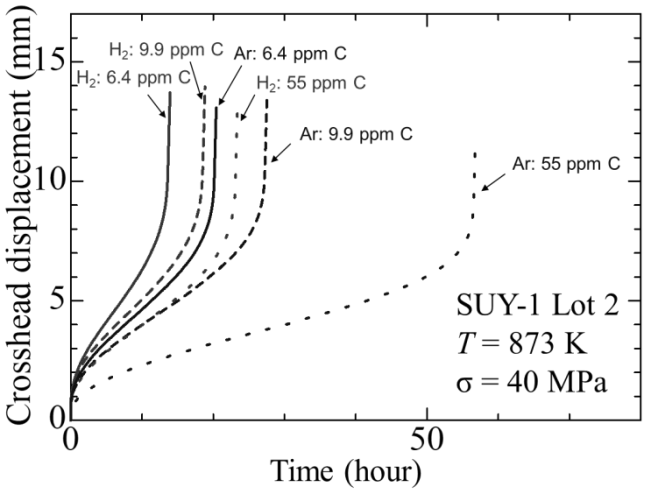


747

748 Fig. 154. Carbon content in the specimen Lot 1 before and after creep testing.

749

750



751

752 Fig. 1~~5~~6. Effect of carbon and hydrogen on creep deformation of Lot 2.

753

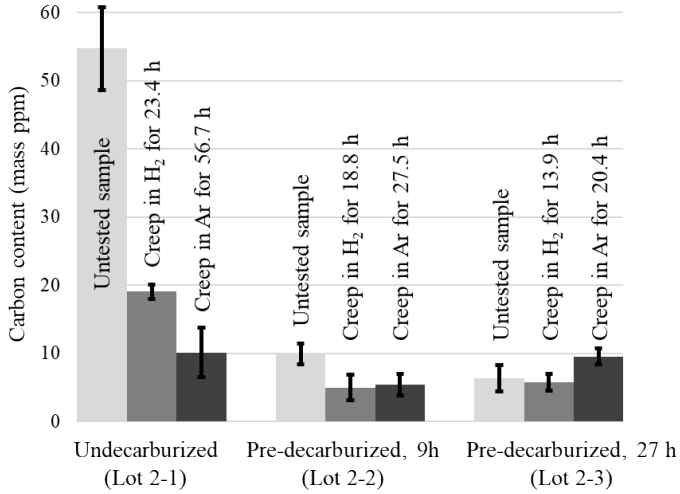


Fig. 1~~6~~7. Change in carbon content of the un-decarburized specimen (Lot-2-1) and pre-decarburized specimens (Lot 2-2 and Lot 2-3) before and after creep testing under 40 MPa stress in hydrogen and argon atmospheres.

761 Table 1 High-temperature hydrogen devices and their operating temperatures

Device	Purpose	Temperature [~~°C~~K]
Solid oxide fuel cell (SOFC)	Power generation	~~500~~773~~-750~~-1023 (Intermediate-temp. SOFC) ~~850~~1123~~-1000~~-1273 (High-temp. SOFC) [1)]
Solid oxide electrolysis cell (SOEC)	H_2 production	~~600~~873~~-900~~-1173 [2)]
H_2 gas turbine	Power generation	~~1200~~1473~~-1650~~-1923 [3)]
H_2 engine	Motive power	
High temperature gas cooled reactor (HTGR)	H_2 production	~~750~~1023~~-950~~-1223 [4)]
Methanation	Fuel synthesis	~~150~~423~~-550~~-823 [5)]
Sustainable aviation Fuel (SAF)	Fuel synthesis	>~~120~~393* [6)]
H separation from NH_3	H_2 production	>~~327~~600** [7)]
H-reduction steelmaking	Steel production	>~~1400~~1673*** [8)]
H_2 boiler	Heat generation	
H_2 hot water supply		

762 * Varies depending on the synthesis method

763 ** Varies depending on the catalyst

764 *** Considered to be comparable to that of a conventional blast furnace

765

766 Table 2 Chemical composition of the SUY-1 in as-received condition (mass %)

	C*	Si	Mn	P	S	Cu	Ni	Cr	Fe
Lot 1	0.0046	Trace	0.24	0.005	0.004	N/A	0.01	0.02	Bal.
Lot 2	0.0055	0.01	0.25	0.006	0.004	0.01	0.01	0.02	Bal.

767 *Measured by infrared adsorption method. Other elements are from material certificate.

768

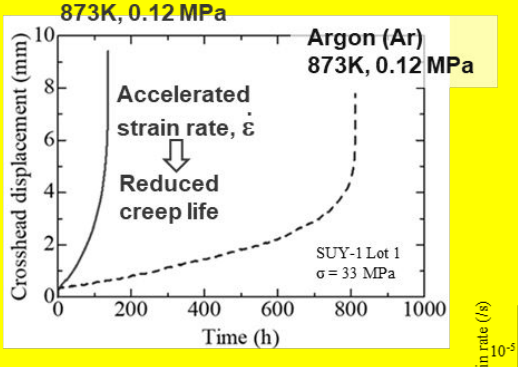
769 Table 3. Mechanical properties of the SUY-1 Lot 1

Temperature (K)	0.2% proof strength, $\sigma_{0.2}$ (MPa)	Ultimate tensile stress, UTS (MPa)	Elongation, δ (%)	Reduction of area, ϕ (%)
293	188	297	43	92
873	121	122	18	99

770

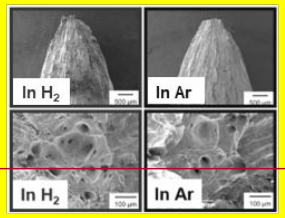
Effect of hydrogen on creep properties of pure iron

Hydrogen (H_2)
873K, 0.12 MPa

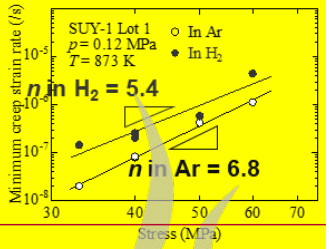


$\dot{\varepsilon}$

SUY-1 Lot 1
σ = 33 MPa



Hydrogen accelerates creep without altering its fundamental mechanism.



Stress exponent, *n*

Similar fracture profile & fracture surface

$$\dot{\varepsilon} = A\sigma^n \exp(-\frac{Q_c}{RT})$$

n

Power-law creep

Hydrogen-reduced creep activation energy, *Q*c

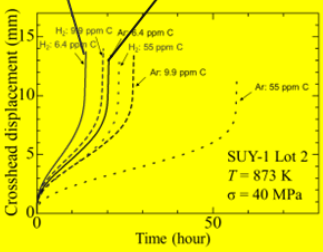
Vacancy formation energy is reduced by hydrogen.

Enhanced dislocation climb

Accelerated creep strain rate

Pre-decarburized, H_2, 873K, 0.12 MPa

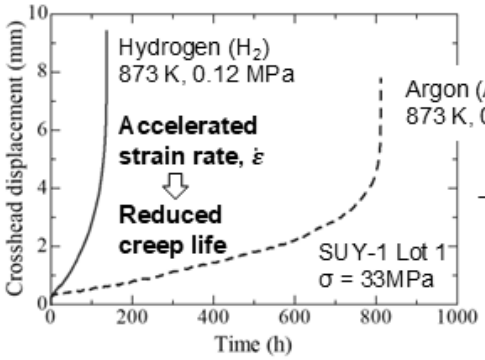
Pre-decarburized, Ar, 873K, 0.12 MPa



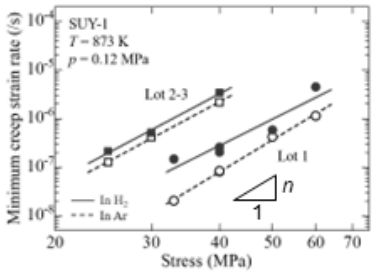
Decarburization reduces creep life, but hydrogen acts independently to further accelerate creep.

772

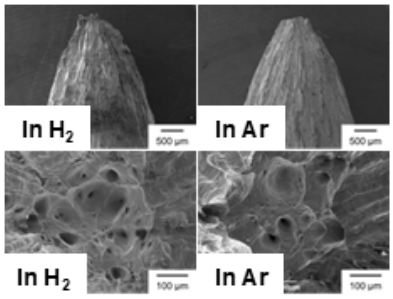
Effect of hydrogen on creep properties of pure iron



$\dot{\varepsilon}$



Pre-decarburized material
Stress exponent $n \simeq 6$ both in H_2 and Ar ⇨ **Power-law creep**

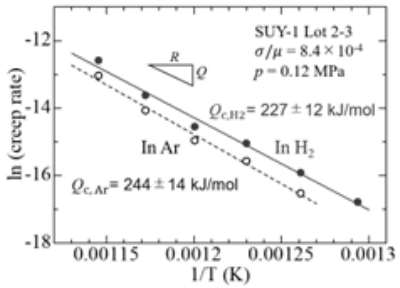


SUY-1 Lot 1, σ = 33MPa

Similar fracture profile & fracture surface

⇩

Hydrogen accelerates creep without altering its fundamental mechanism.



Creep activation energy Q_c may be lower in hydrogen than in argon.

$$\dot{\varepsilon} = A\left(\frac{\sigma}{E}\right)^n \exp\left(\frac{Q_c}{RT}\right)$$

Hydrogen accelerates creep strain rate by lowering creep activation energy Q_c.

⇩

Mechanism:

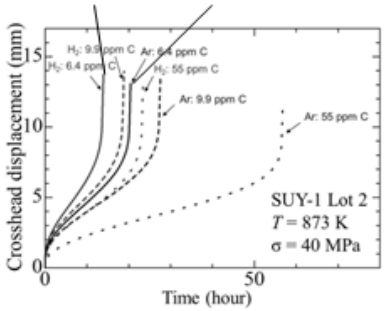
Vacancy formation energy is reduced by hydrogen.

⇨ **Enhanced dislocation climb**

⇨ **Accelerated creep strain rate**

Pre-decarburized H_2, 873 K, 0.12 MPa

Pre-decarburized Ar, 873 K, 0.12 MPa



Decarburization reduces creep life, but hydrogen acts independently to further accelerate creep.

775

776 **Graphical Abstract**

777